Entropy Production in the Active Ising Model

Lauren Paonessa
*Graduate Program in Biophysics, Harvard University, Cambridge MA, 02138
(Dated: Dated: May 17, 2024)

Irreversibility is a distinguishing feature of non-equilibrium systems. The entropy production rate (EPR) quantifies the breakdown of time-reversal symmetry, providing a metric to assess the strength of the non-equilibrium nature of different regions of phase space. In this paper, we measure the EPR in the Active Ising Model (AIM), across it's phase diagram with two approaches: the Kullback-Leiber divergence (KLD) and integrating the local entropy production. We derive local entropy production of the AIM from the hydrodynamic equations. We study the performance of the two EPR measurement methods across the phase diagram of the AIM and assess their agreement and breakdown. Lastly, we examine the microscopic sources of the EPR with the KLD.

I. INTRODUCTION

Active matter systems, defined as assemblies of interacting particles that consume energy to move or exert mechanical work, exhibit a variety of exotic collective behaviours [1–3]. Among them, a remarkable phenomena called collective motion, where large groups undergo coherent displacements over scales much larger than individual particles [1–3]. Similar behaviour is observed in living material such as bacterial colonies, biological tissues or bird flocks [1, 2]. The field of active matter provides insight into the key ingredients necessary to generate various collective phenomena often similar to those observed in nature [1–3].

The question has often been raised if non-equilibrium systems can be mapped to equilibrium models, as often coarse-grained behaviours of the latter classes of systems appears similar to the eye [4, 5]. For the parameter regimes where collective phenomena is observed, such as flocking in d=2, there is no corresponding equilibrium system [5, 6]. Irreversibility, an explicit violation of equilibrium, is the key ingredient for collective phenomena [5]. A commonly used measure for quantifying the extent of the deviation from equilibrium is the entropy production rate (EPR) [2, 5]. In the literature, this quantity is calculated from both the dynamical mean-field and single particle descriptions of a system [4, 7, 8].

In this paper, we investigate the EPR of the Active Ising Model (AIM) with metric alignment [6]. This model was presented as an alternative strategy to gain insight into the flocking, while circumventing the analytical and numerical challenges of the Viseck model [6]. This model contains the two key features for flocking: self-propulsion and aligning-interactions [6]. First, we present the microscopic model and coarse-grain to the mean-field model with fluctuations. We then present two methods to calculate the EPR, at the single trajectory level using Kullback-Leiber divergence (KLD), and at the hydrodynamic level by deriving an analytical expression for the local EPR. We then compare the EPR calculated from both methods across the AIM phase diagram. We observe good agreement between the scaling of the EPR measures near the onset of flocking. Additionally, leveraging the Markovian nature of the AIM, we examine the contribution of different microscopic sources to the EPR.

II. THE ACTIVE ISING MODEL

A. Definition of the Microscopic Model

We consider N particles on a 2D lattice of with $L_x \times L_y$ sites with periodic boundary conditions. Each particles carries a ± 1 spin and there are no restrictions on the occupancy number of particles per site. There may be $n_i^{\pm}$ particles with ± 1 spins on a given site $i \equiv (i_x, i_y)$. The local density and magnetization per site is defined as $\rho_i = n_i^+ + n_i^-$ and $m_i = n_i^+ + n_i^-$. We consider a continuous time Markov model where the particles hop between sites with a biased diffusion and flip between spin states depending on the local magnetization of the site [6]. The rates of these processes are described in Fig.1, and imbue the system with the key ingredient necessary for flocking: self-propulsion and self-alignment [6].

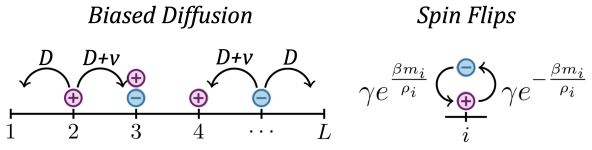

FIG. 1. Schematic of the AIM actions and their associated rates. The particle hopping will have a bias along the x-axis based on it's spin. The particle spin will flip at a rate dependent on the magnetization of the site it's on. This rate encodes the self-alignment property of the system. Adapted from Ref. [6].

B. Hydrodynamic Description of the AIM: The Refined Mean-Field Model

The simplest route to an analytical treatment of the AIM is via the mean-field approximation. To construct this model, we consider non-interacting particles whose

orientations experience an external field $\overline{m}(\mathbf{r})$ that modulates alignment. In the mean-field, we define this field with respect to $m(\mathbf{r})$, and $\rho(\mathbf{r})$ depending on the type of alignment interactions [6]. The dynamics then becomes decoupled and we consider the evolution of the one-body density $P(\mathbf{r}, \sigma, t)$ [9] to find a particle at a given location $\mathbf{r}$ at time t with spin σ,

$$\begin{aligned}\partial_t P(\mathbf{r},\sigma,t) =& D\nabla^2 P(\mathbf{r},\sigma,t) + \partial_x[v((r),\sigma,t)] \\ &- e^{\beta\sigma\overline{m}(\mathbf{r})}P(\mathbf{r},\sigma,t) + e^{\beta\sigma\overline{m}(\mathbf{r})}P(\mathbf{r},\sigma,t)\end{aligned} \tag{1}$$

where we have set γ to 1 without loss of generality. Then in the same spirit as in the microscopic model, we introduce the one-body magnetization and density fields [9], $m(\mathbf{r},t) = P(\mathbf{r},1,t)$ - $P(\mathbf{r},-1,t)$ and $\rho(\mathbf{r},t) = P(\mathbf{r},1,t) + P(\mathbf{r},-1,t)$, respectively. Then, using Eqn. 1 we obtain,

$$\begin{aligned}\partial_t =& D\nabla^2\rho - \partial_x(vm) \\ \partial_t m =& D\nabla^2 m - \partial_x(v\rho) - \mathcal{F}(\rho,m,\overline{m})\end{aligned} \tag{2}$$

where $\mathcal{F}(\rho, m, \overline{m})$ is given by,

$$\mathcal{F}(\rho,m,\overline{m}) = 2\rho sinh(\beta\overline{m}) - 2mcosh(\beta\overline{m}) \tag{3}$$

In the case of metric alignment, we set

$$\overline{m}(\mathbf{r}) = \frac{m(\mathbf{r})}{\rho(\mathbf{r})} \tag{4}$$

In previous work by Solon et al. [6], it was shown that this mean-field fails to correctly capture the first-order nature of the transition to collective motion. This behaviour was recovered by adding density dependent fluctuations to the magnetic field evolution [6] yield a Refined-Mean Field Model (RMFM) of the AIM,

$$\begin{aligned}\partial_t =& D\nabla^2\rho - \partial_x(vm) \\ \partial_t m =& D\nabla^2 m - \partial_x(v\rho) - \mathcal{F}(\rho,m) + \sqrt{2\sigma\rho}\eta\end{aligned} \tag{5}$$

where η is Gaussian white noise with variance $\langle\eta(\mathbf{x},t)\eta(\mathbf{y},t')\rangle = \delta(\mathbf{x}-\mathbf{y})\delta(t-t')$ and σ modulates the strength of the fluctuations.

Note, in this model explicit fluctuations in density are neglected. The addition of this fluctuation term was deemed sufficient to recover the first-order phase transition behaviour [6]. We will use this RMFM to analytical derive the local EPR of the AIM.

III. ENTROPY PRODUCTION RATE (EPR)

The EPR quantifies the irreversibility of a system [5]. According to stochastic thermodynamics [2], the EPR is defined as,

$$\dot{S} = \lim_{\tau\to\infty}\frac{1}{\tau}\left\langle ln\frac{\tilde{P}_F[\phi(\mathbf{r})]}{\tilde{P}_R[\phi(\mathbf{r})]}\right\rangle \tag{6}$$

where $\tilde{\mathcal{P}}$ and $\tilde{\mathcal{P}}^R$ is the probability of a path $\{\phi[\phi(\mathbf{r},t)]\}_{0\le t\le\tau}$ and it's time-reversed path. The average is over noise realization, which under the assumption of ergodicity can be replaced with the average over a long trajectory [4]. We present and apply two different methods to calculate EPR in the AIM.

A. Entropy Production Rate from Single Trajectories

The irreversibility of an active matter system is present at the level of a single particle [6, 7]. This is clear from the move rates of the AIM illustrated in Fig.1. The forward move rates do not equal the backward move rates, encoding time reversal symmetry breaking (TRS) into the microscopic model. The signature of TRS is macroscopic entropy production. The connection between entropy production and irreversiblity is defined through the Kullback-Leiber divergence (KLD) [7]. The KLD measures the distinguishability of two probability distributions $p(x)$ and $q(x)$,

$$D[p(x)||q(x)] = \int dx p(x) log\frac{p(x)}{q(x)} \tag{7}$$

This quantity is always positive and disappears when $p(x)$ equals $q(x)$ [7].

The distinguisability of a process and it's time reversal can be quantified with KLD, yielding a measure of the irreversibility. Consider a process in which the system has reached a non-equilibrium steady state, the entropy production per unit time $\dot{S}$ can be expressed in terms of the path probability of the forward $\{z(t)\}_{t=0}^{\tau}$ and backwards $\{\tilde{z}(\tau-t)\}_{t=0}^{\tau}$ trajectories,

$$\langle\dot{S}\rangle = \lim_{\tau\to\infty}\frac{k}{\tau}D[\tilde{\mathcal{P}}(\{z(t)\}_{t=0}^{\tau})||\tilde{\mathcal{P}}(\{\tilde{z}(\tau-t)\}_{t=0}^{\tau})] \tag{8}$$

KLD completely describes the EPR when the entire microscopic trajectory is considered [7]. However, if only some observables of the system are considered in the trajectory, the KLD provides a lower bound on the EPR [7]. This presents the potential to explore the contribution of different observables to the EPR.

For a Markovian process, the KLD rate can be calculated for each individual step [7]. The KLD rate for the process bounds en entropy production from below in the limit of long sampling times [7]. The m-th order KLD of a random process $\mathcal{X}$ can be calculated from a single trajectory, $x_1^n = (x_1, ..., x_n)$, and it's reverse, $x_n^1 = (x_n, ..., x_1)$,

$$\begin{aligned}\mathcal{D}_m^X =& \mathcal{D}[p(x_1^n)||p(x_n^1)] \\ =& \sum_{i=0}^{n} p(x_i\to x_{i+1}) log\frac{p(x_i\to x_{i+1})}{p(x_{i+1}\to x_i)}\end{aligned} \tag{9}$$

This quantity can then be used to define a lower bound for the EPR per step,

$$\langle \dot{S} \rangle \geq k \lim_{n\to\infty} \frac{\mathcal{D}_n^X}{n} \tag{10}$$

This becomes an equality when the random variable samples the entire description of microstate of the system [7].

We use this discrete summation to calculate the EPR in AIM simulations, where forward and backward step probabilities can be exactly computed from the microscopic rates. The generalized rates for the time-reversal asymmetric moves are detailed in Fig.2.

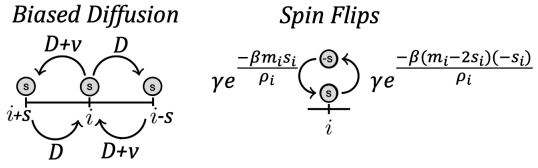

FIG. 2. The generalized forward and backwards rates for each time-reversal asymmetric step. These expressions were used in the AIM simulation to store the forward and reverse rates for each step of a selected particle.

B. Local Entropy Production Rate of the AIM

In previous work by Nardini et al. [4], the EPR of a system self-propelling particles exhibiting motility induced phase separation (MIPS) was was decomposed locally (in real space). This allowed for the study of the EPR spatial structure. In the phase separated state, they observed EPR concentrated mainly on interfaces with bulk contributions tending to zero in the low noise limit [7]. Motivated by this work, we seek to derive a similar formula for the AIM with the aim of potentially studying the spatial structure of the EPR in the flocking phase.

According to field theory methods [2, 4], the path weight can be written as,

$$\begin{aligned} \tilde{\mathcal{P}}[\phi] &= exp[-\mathcal{A}^F] \\ \tilde{\mathcal{P}}_R[\phi] &= exp[-\mathcal{A}^R] \end{aligned} \tag{11}$$

The EPR calculation can be written as [2, 4],

$$\dot{S} = \lim_{\tau\to\infty} \frac{\mathcal{A}^R - \mathcal{A}^F}{\tau} \tag{12}$$

We will then write the entropy production as a sum over local spatial contributions as,

$$\dot{S} \equiv \int d\mathbf{r} \sigma_\phi(\mathbf{r}) \tag{13}$$

where σ_ϕ can be view as as the local EPR [2, 4].

To identify the relevant dynamical action of the AIM for EPR calculation, we recall that the probability of a given path depends on the probability of the noise realization yielding that path [2]. The probability of a given Gaussian white noise realization $\{\eta(t')\}$ is,

$$\tilde{\mathcal{P}}[\{\eta(\mathbf{r},t)\}] \propto exp\left[-\frac{1}{2}\int d\mathbf{r}dt\eta^2\right] \tag{14}$$

We can express η in terms of the density and magnetization field using Eqn 5.,

$$\eta(\mathbf{r},t) = \frac{1}{\sqrt{2\sigma}\rho}\left[\dot{m} - D\nabla^2 m + v\partial_x\rho + \mathcal{F}(\rho,m)\right] \tag{15}$$

This allows us to define the forward and reverse path probabilities of the magnetic field [2], $\{m(\mathbf{r},t)\}$, at a given position r after time t,

$$\begin{aligned} \tilde{\mathcal{P}}[\rho,m]^F, R \propto & exp\left[-\frac{1}{4\sigma}\int dt \frac{1}{\rho^2}(\pm\dot{m} - D\nabla^2 m \right. \\ & \left. + v\partial_x\rho + \mathcal{F}(\rho,m))^2\right] \\ = & exp[-\mathcal{A}_{F,R}] \end{aligned} \tag{16}$$

where we have identified the forward and reverse dynamical actions, $\mathcal{A}_F$ and $\mathcal{A}_B$.

We can now subtract $\mathcal{A}_F$ from $\mathcal{A}_B$ and we obtain,

$$\dot{S} = -\lim_{\tau\to\infty}\int d\mathbf{r}dt \frac{1}{\sigma}\frac{\dot{m}}{\rho^2}[D\nabla^2 m - v\partial_x\rho - \mathcal{F}(\rho,m)] \tag{17}$$

From here, we can identify the local EPR of the AIM,

$$\sigma_m(\mathbf{r}) = -\frac{1}{\sigma}\left\langle \frac{\dot{m}}{\rho^2}[D\nabla^2 m - v\partial_x\rho - \mathcal{F}(\rho,m)]\right\rangle \tag{18}$$

Notably, this derivation of local EPR neglects any contributions due to density fluctuations [2].

IV. RESULTS

A. Global Entropy Production

We explored the simulation space of the AIM and measured the EPR. The trajectory EPR is recorded from each move of a single particle. The RMFM EPR is computed for each microscopic step at each lattice site, then summed over lattice sites. Both EPR recordings started after an apparent steady state was reached.

The trajectory based approach to computing EPR is a well-established method that does not have employ any parameter-space dependent approximation in it's construction. For this reason, we assume this EPR is a closer measure to the ground-truth EPR. We shall compare the scaling of the global EPR measured from the analytic expression for the EPR to that of the trajectory EPR to assess it's validity.

First, we validate our trajectory EPR measurement by examining the scaling of the AIM in the limit of $\frac{v}{D} << 1$,

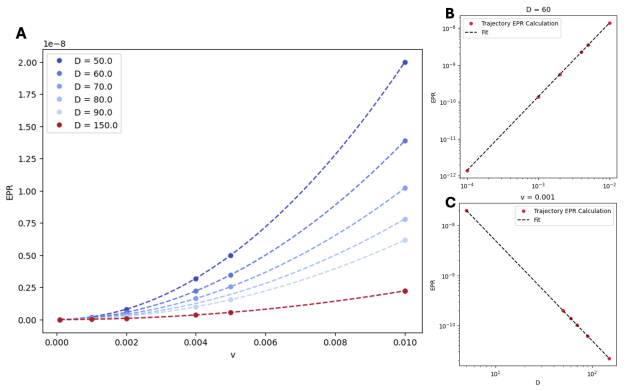

FIG. 3. AIM EPR scaling in the limit $\frac{v}{D} << 1$ measured from a single particle trajectory. **A**) This graph illustrates the EPR scaling with the speed, v, and diffusion coefficient, D. **B**) The scaling with v fit with a linear fit slope of 2 for D=60. **C**) The scaling with D fit with a linear fit slope of 2 for v=0.001. Simulation parameters: $L_x \times L_y = 200 \times 200$, ρ=0.00001, T= 15, γ=0.

and $\gamma = 0$, where it behaves as a run-and-tumble particle (RTP) system. The EPR is solely from the biased diffusion of particles and assumes a straightforward scaling,

$$\langle \dot{S} \rangle \propto \frac{v+D}{v+2D} log\left(\frac{v+D}{D}\right) + \frac{D}{v+2D} log\left(\frac{D}{D+v}\right) \approx \left(\frac{v}{D}\right)^2 \tag{19}$$

This scaling relation was recovered from the trajectory EPR calculations, this is detailed in Fig. 3.

After numerical validation of our EPR trajectory calculation, we studied EPR across the phase diagram of the AIM. We varied ρ and measured the EPR in all three phases of the AIM, this is illustrated in Panels A and B in Fig. 4.

In Panel C in Fig. 4., the EPR calculated using the two different methods are plotted with respect to ρ. We see that at low densities and around the flocking phase ($\rho = 4$), the EPR scalings are qualitatively similar. However, we see a stronger drop off in the RMFM EPR, likely due to the vanishing magnetization at low densities. This leaves the biased diffusion as the main contributor to the EPR, however, this behaviour is not capture by the RMFM. The EPR agreement near the critical point is reasonable as the RMFM has been reported to describe the transition to flocking correctly, suggesting in this regime it describes the AIM well. We see deviations between the models at high densities, this is likely due to the $\frac{1}{\rho^2}$ scaling of σ_m, rapidly decreasing the RMFM EPR. Repeating this measurement at higher temperatures would permit the EPR in the three phases to be measured at high densities which could potentially decrease the effect of this scaling. This could result in improved agreement of the models at higher densities,

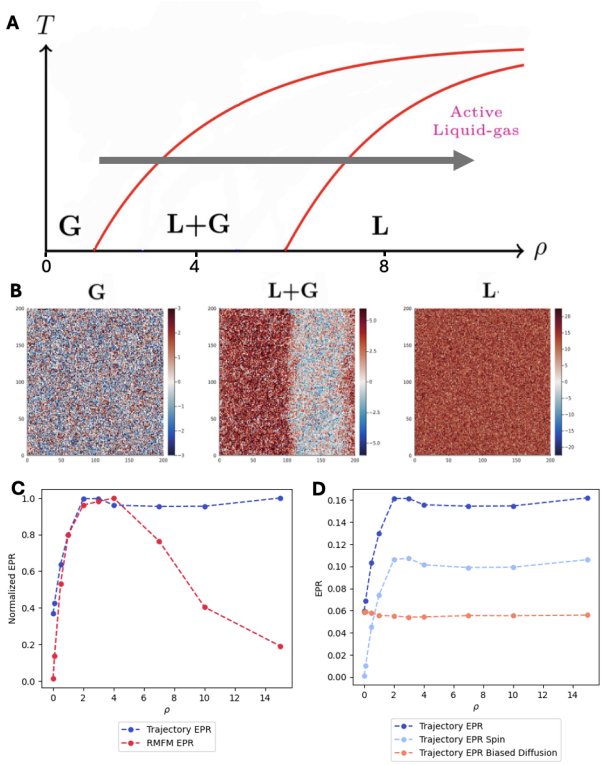

FIG. 4. **A**) Schematic depiction of simulation procedure wherein the EPR was measured as a fixed $T = 0.6$ and varying ρ across the AIM phase diagram. Adapted from Ref. [6]. **B**) Snapshots of systems samples across the phase diagram of the AIM. From left to right, $\rho = 1, 4, 8$. **C**) The normalized EPR calculated from the trajectory and RMFM equation. These plots were normalized to compare the scaling. **D**) The microscopic breakdown of the EPR from the trajectory calculation. Simulation parameters: $L_x \times L_y = 200 \times 200$, D=1, v=0.6, γ=1.

after the transition to the ordered liquid phase.

In Panel D in Fig. 4., we breakdown the contributions of the two microscopic sources of irreversibility in the AIM. This can easily be done by isolating the spin flip steps and the biased diffusion steps in the trajectory of an AIM particle and using Eqn. 10. for each set and normalizing by the total number of steps. This analysis suggests that the driving force for the increase in the EPR in the banding phase is the spin flipping. The biased diffusion appears to impose a baseline level of EPR in the regime we have examined, such that even at low densities we do not have an equilibrium gas model. Extending this curve to investigate higher densities, though computationally costly, could provide more insights into the EPR driving forces in the flocking phase. It is worth noting that this graph captures the central statement of the KLD, that as microsopic degrees of freedom are integrated out of the probability distributions used to compute KLD, their measured distinguishability decreases.

V. CONCLUSION

We present two approaches to calculating the EPR in the AIM: from a single particle trajectory level and analytically from the mean-field hydrodynamic AIM equations with fluctuations. After validating our trajectory EPR calculation, we examine the microscopic breakdown of the trajectory EPR and the agreement between the two EPR measurements with varying ρ. The breakdown of the trajectory EPR appears to suggest that spin flipping accounts for the increase in EPR near the onset of flocking. We observed good agreement between the EPR scaling of these two approaches with ρ near the onset of near in the banding phase. This may suggest that the expression for σ_m is a good approximation to the local EPR near the critical point. In lieu of these results, in future works the spatial structure of the σ_m could be studied in the banding phase. Ideally, the measurements for σ_m would be stored such that the center of the band remained fixed in space. It would be interesting to see if, similar to MIPS [4], the EPR is concentrated near interfaces and if potentially the front and the back of the band would have distinct EPR signatures. Furthermore, a more extensive and densely-sampled sweep of the EPR throughout parameter space would provide further insights into the regimes where irreversibility is a dominant feature of the AIM.

VI. ACKNOWLEDGEMENTS

I would first and foremost like to thank Sunghan Ro for guiding my through this project. His mini lectures and willingness to respond to emails and meet truly made this project a very interactive and fun learning experience for me. Next, I would like to thank Mehran Kardar for a great semester of the most challenging yet conceptually interesting physics material I have ever encountered. I look forward to noticing the subtle signatures of universality in my future theoretical and experimental work. Lastly, I would like to thank Seth Musser for his invaluable office hours and talents in explaining complex concepts in a intuitive manner.

[1] O. Granek, Y. Kafri, M. Kardar, S. Ro, A. Solon, and J. Tailleur, Inclusions, Boundaries and Disorder in Scalar Active Matter (2023), arXiv:2310.00079 [cond-mat].
[2] M. E. Cates, Active Field Theories (2019), arXiv:1904.01330 [cond-mat].
[3] M. J. Bowick, N. Fakhri, M. C. Marchetti, and S. Ramaswamy, Symmetry, Thermodynamics and Topology in Active Matter (2021), arXiv:2107.00724 [cond-mat].
[4] C. Nardini, Fodor, E. Tjhung, F. van Wijland, J. Tailleur, and M. E. Cates, Entropy Production in Field Theories without Time-Reversal Symmetry: Quantifying the Non-Equilibrium Character of Active Matter, Physical Review X **7**, 021007 (2017), publisher: American Physical Society.
[5] F. Ferretti, S. Grosse-Holz, C. Holmes, J. L. Shivers, I. Giardina, T. Mora, and A. M. Walczak, enSignatures of irreversibility in microscopic models of flocking, Physical Review E **106**, 034608 (2022).
[6] A. P. Solon and J. Tailleur, Flocking with discrete symmetry: the 2d Active Ising Model, Physical Review E **92**, 042119 (2015), arXiv:1506.05749 [cond-mat].
[7] Roldán and J. M. R. Parrondo, Entropy production and Kullback-Leibler divergence between stationary trajectories of discrete systems, Physical Review E **85**, 031129 (2012), arXiv:1201.5613 [cond-mat].
[8] S. Ro, B. Guo, A. Shih, T. V. Phan, R. H. Austin, D. Levine, P. M. Chaikin, and S. Martiniani, enModel-Free Measurement of Local Entropy Production and Extractable Work in Active Matter, Physical Review Letters **129**, 220601 (2022).
[9] D. Martin, G. Spera, H. Chaté, C. Duclut, C. Nardini, J. Tailleur, and F. van Wijland, Fluctuation-Induced First Order Transition to Collective Motion (2024), arXiv:2402.05078 [cond-mat].